# Table of Contents

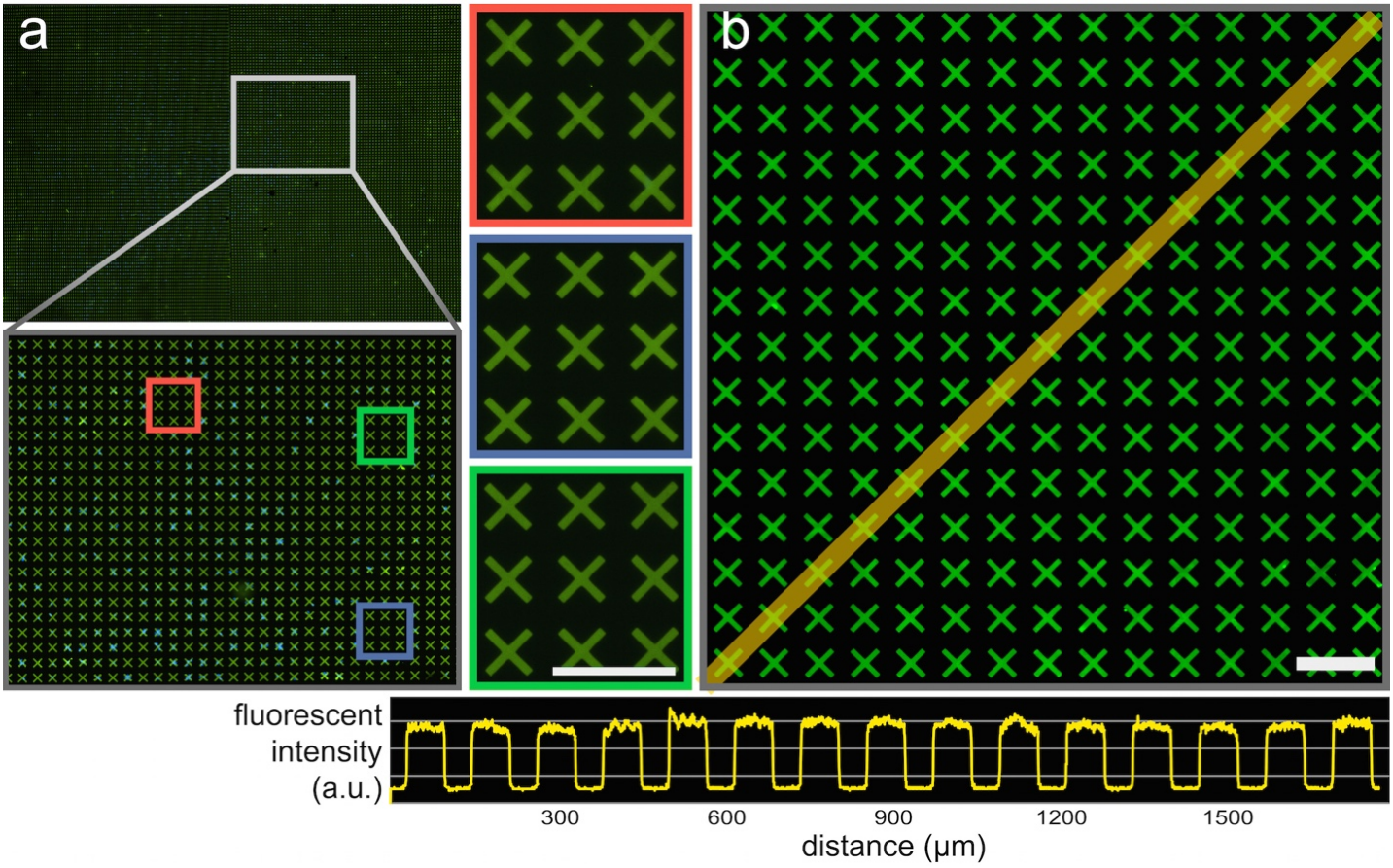


**Figure S1: Reproducibility of biomolecule patterning via sacrificial dextran layers.**

(a) Multiple regions within a substrate blown-up, qualitatively demonstrating repeatability and consistency of patterns prepared using our sacrificial dextran layer approach. Defects in patterns are rare, occurring in <1% of patterns, as determined by inspecting 625 individual patterns in a 25 by 25 pattern square region. (b) Line-scan of fluorescent intensity of 15 adjacent cross patterns (70μm diagonal) demonstrating the uniformity of pattern transfer. In this substrate, equal parts of fibronectin and Alexa Fluor 488-conjugated fibrinogen were patterned. Image was taken with 10x magnification using 1 s exposure. Scale bars represent 150 μm.

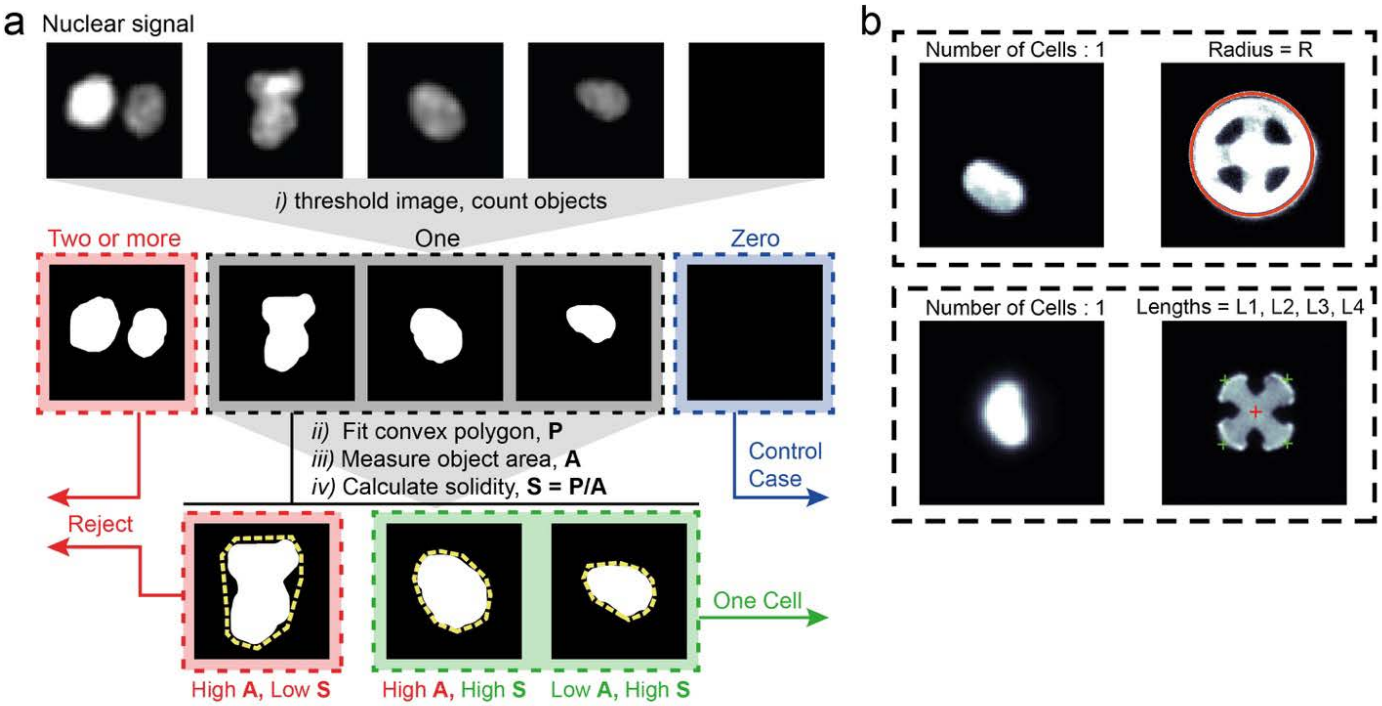


**Figure S2: Cell counting algorithm and data storage.**

(a) Algorithm used to count cells adhered to a single pattern. The input image is thresholded and the independent objects present in the frame are counted. Images with counts of >1 and 0 are classified appropriately, while those with counts of exactly 1 have the smallest possible convex polygon (P) fitted to the object, and the fraction of the area of this polygon (P) that is occupied by the object area (A), called 'solidity' (S=P/A) is calculated. Smaller objects are more likely to be a single nucleus. Larger objects are more often multiple nuclei so they must have a high solidity (characteristic of the general shape of a nucleus), to be considered one cell. Using these gates, single objects are sorted with 99% sensitivity and >90% specificity. (b) Representative images of the data stored for each experiment. In addition to a *.mat* file storing the numerical data, an image file is created for every pattern processed in every experiment. This file contains the nuclear signal labeled with the calculated cell count alongside the pattern either overlaid with the circle of best fit in the case of a circular pattern (top) or marked at the center and at each vertex in the case of the cross pattern (bottom). These files are indexed such that they can be specifically looked up or even removed from the data set if they represent noise (e.g. defective pattern).

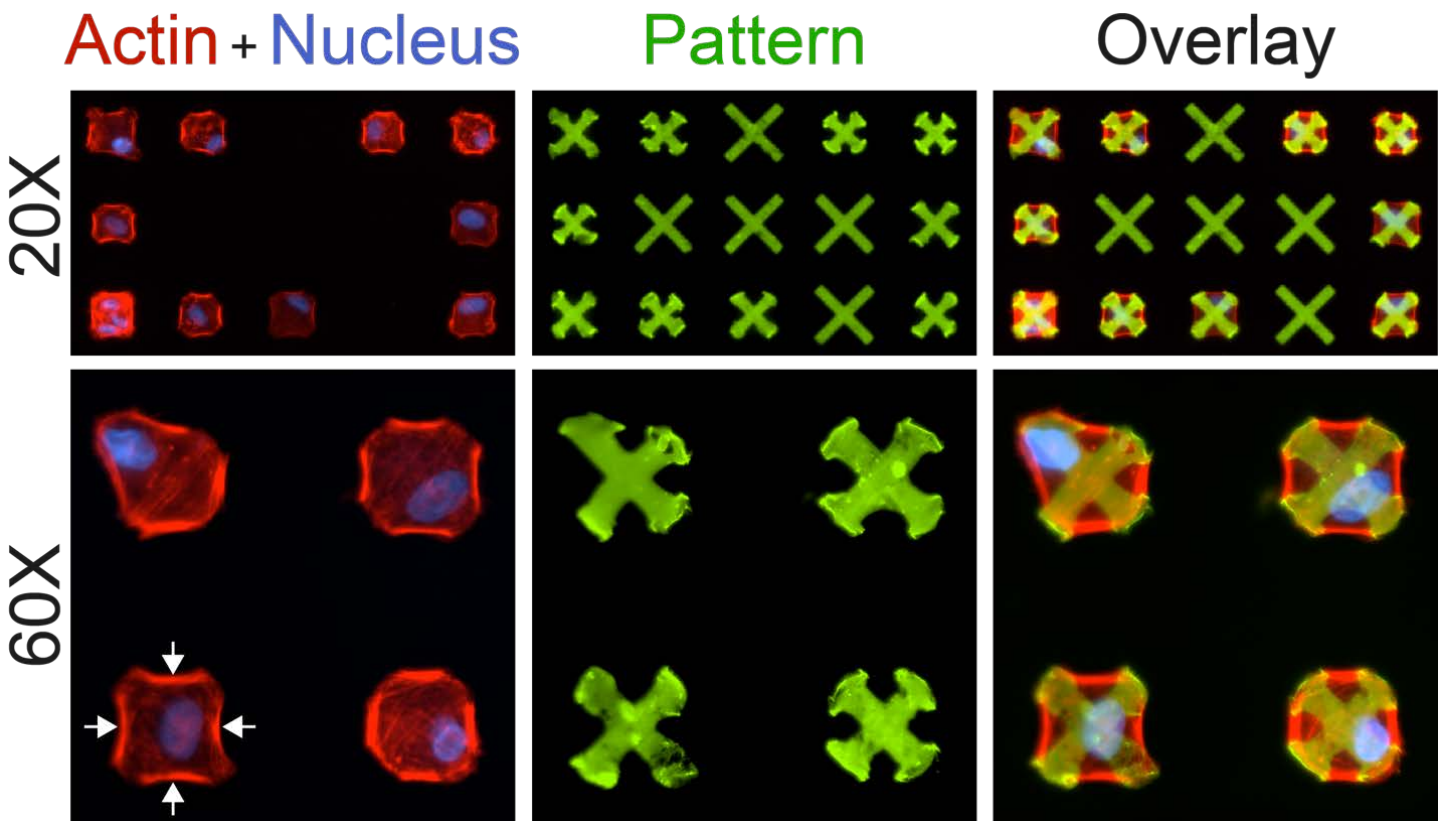


**Figure S3: Actin polarization routes cell forces to pattern vertices.**

Representative fluorescent images of adipose-derived human mesenchymal stem cells adhered to cross patterns (70 μm diagonal, 10 μm bar thickness) consisting of equal parts fibronectin and Alexa Fluor 488 conjugated-fibrinogen. Images of stained actin (red; bound with Alexa Fluor 568-conjugated phalloidin) reveal dense actin networks bridging adjacent pattern vertices (indicated with white arrows), creating tensional symmetries that result in net displacements of the vertices radially inward. Two different fields of view are shown from images taken at either 20X or 60X magnification.

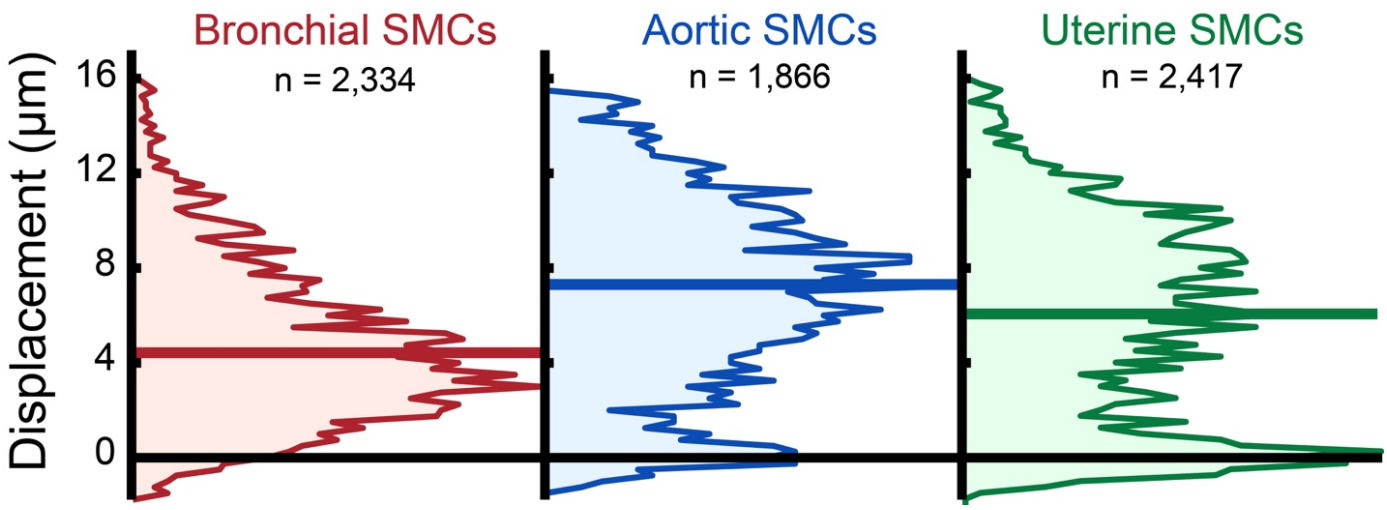


**Figure S4: Contractility of primary human smooth muscle cells.**

Contractility of primary human smooth muscle cells (SMCs) taken from the bronchiole, aorta and myometrium are compared. (a) Aortic and uterine smooth muscle cells demonstrated higher tonal contractile potential than bronchial cells, reflecting the different functions of these tissues despite similar structures. A significant non-contractile population was identified among uterine SMCs perhaps due to contamination by non-SMCs from the site of isolation. This subpopulation may also indicate such cells may exist in multiple phenotypic states e.g. contractile or proliferative. N indicates number of cells in each distribution.

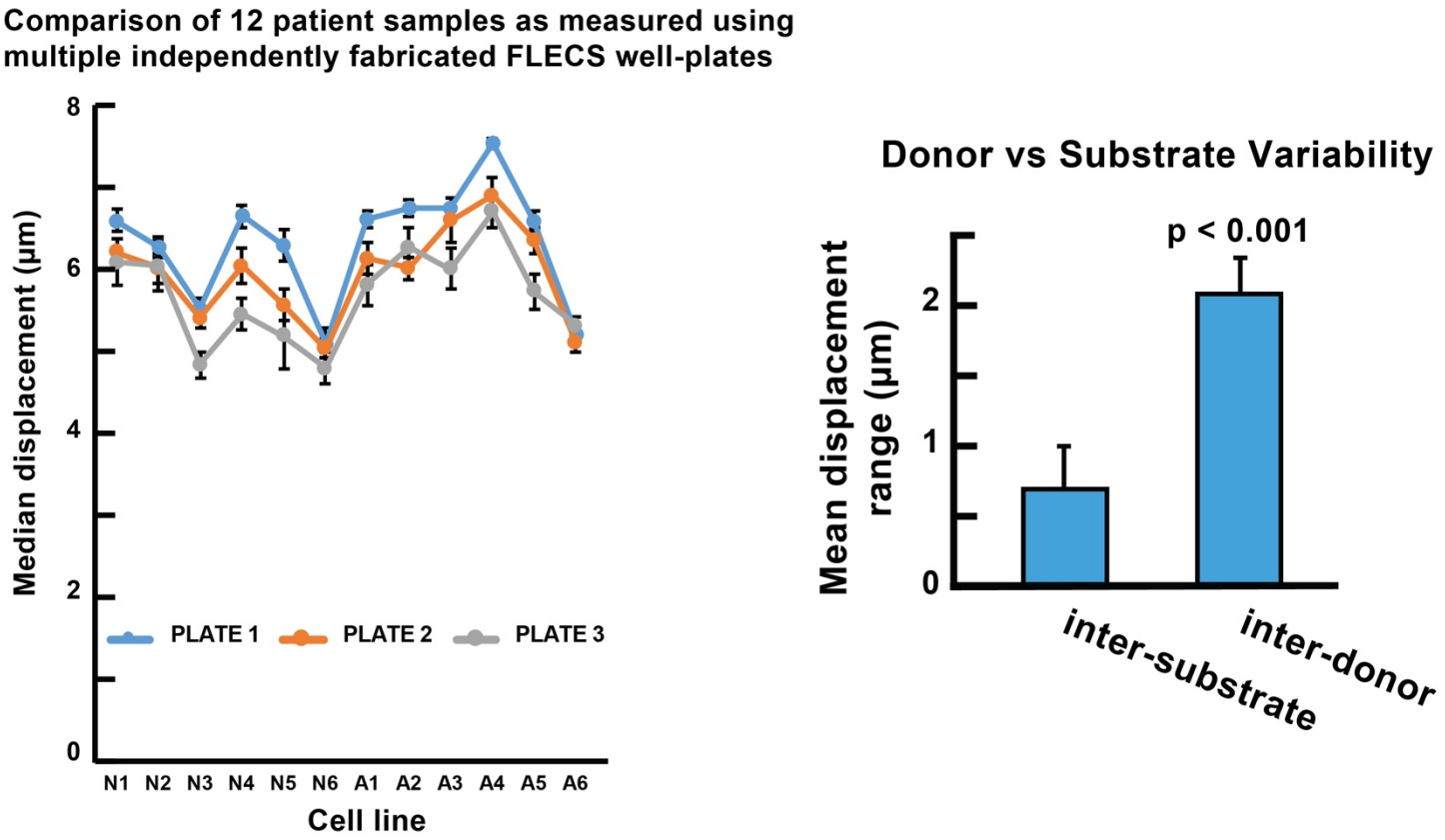


**Figure S5: Measurement variability between donors and substrates**

Twelve patient-derived HASM cell lines were each seeded into 8 wells on 3 separately fabricated FLECS well-plates and their tonic contraction was quantified. The left plot shows the averaged basal tone measurements for each plate and donor. These values are used to quantify both the inter-plate and inter-donor variability and we find the inter-donor (native biological) variability to be significantly larger (right plot) indicating that small variations seen between these substrates do affect the findings and conclusions.

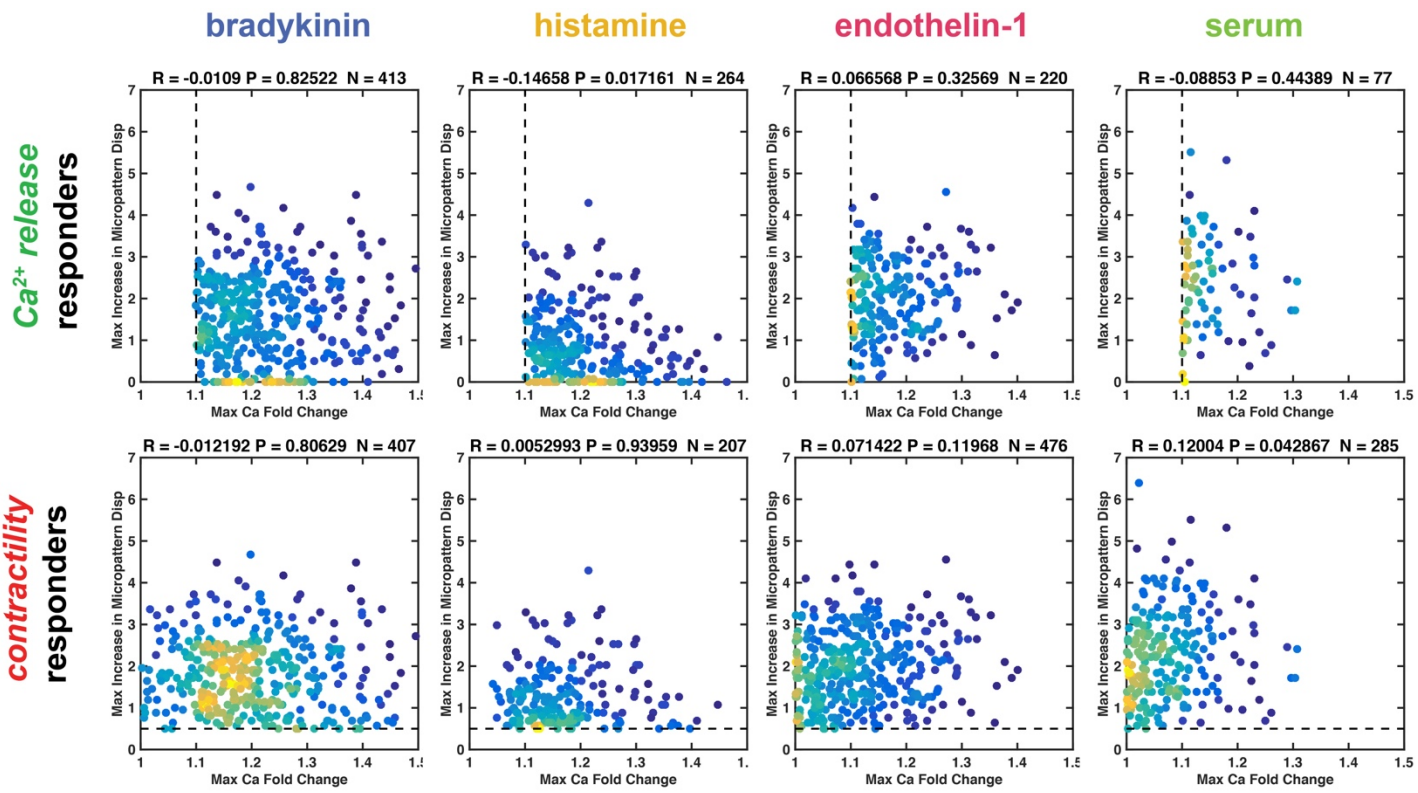


**Figure S6: Simultaneous measurements of calcium release and contractility based on responder gates**

Data from main text Fig. 4 is reanalyzed to consider only robust responders either in terms of calcium signaling (>1.1 intensity change, top row) or in terms of contraction (>1 μm increase, bottom row). After finding little correlation between the two measurements for the ful populations, we tested to see if correlations could be seen when considering robust responders. However, as the plots and Pearson coefficients (top of plot) indicate, even after gating, no significant correlations are observed.

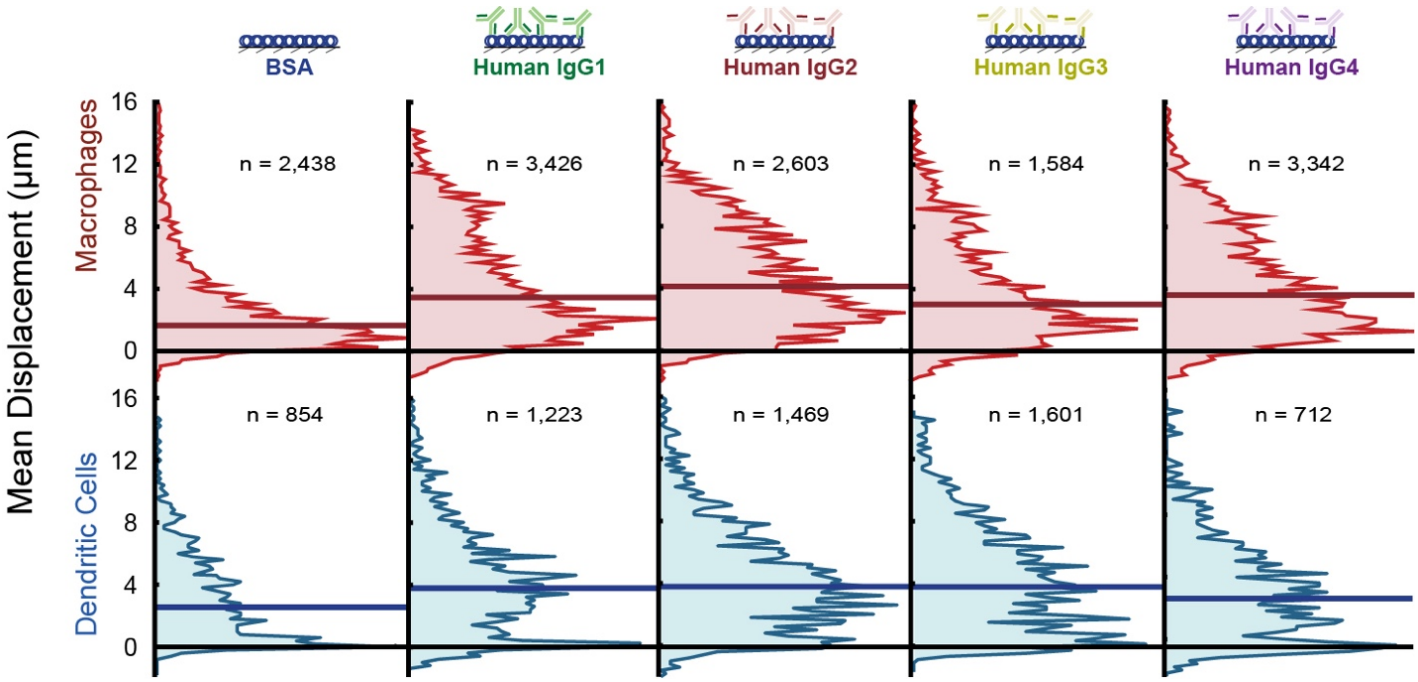


**Figure S7: Comparison of phagocytic forces generated by human monocyte-derived dendritic cells and macrophages engaged in phagocytosis forces.**

Patient-matched monocyte-derived macrophages (MDMs) and dendritic cells (MDCs) on patterns opsonized with various IgG isotypes. Although a greater proportion of MDDCs possessed basal contractile activity than MDMs, their stimulated contractile force generation to all opsonized micropatterns was significantly greater than the non-opsonized controls, and similar to that of MDMs. No obvious differences in force-generation are observed across these isotypes and MDCs are observed to produce forces comparable to MDMs. This results indicate that IgG glycosylation patterns may not greatly contribute to the force-generating steps in phagocytosis.

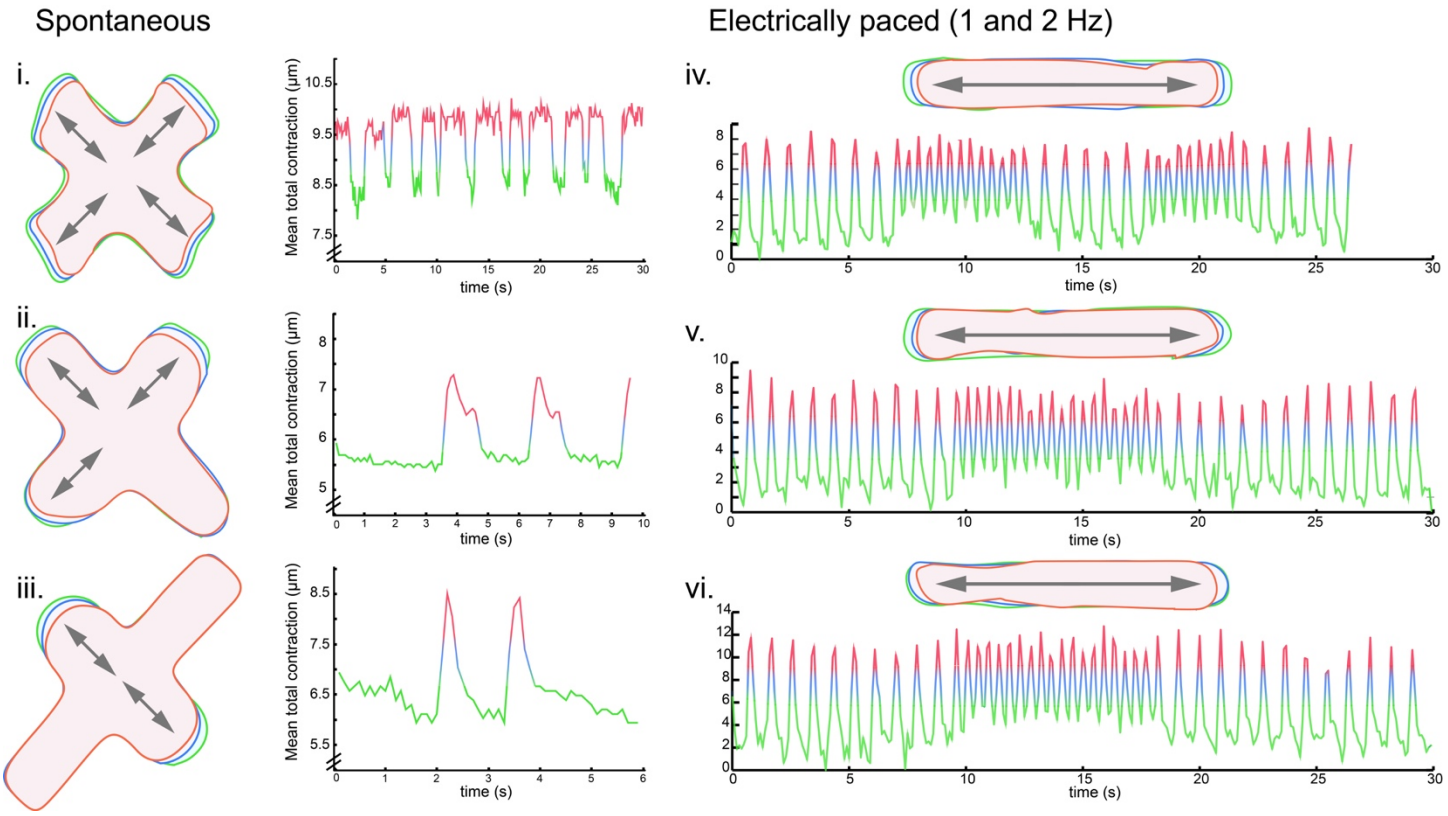


**Figure S8: Traces of live beating single neonatal rat ventricular myocytes.**

Freshly isolated neonatal rat ventricular myocytes seeded on fibronectin-fibrinogen patterns were observed to phasically contract without stimulation approximately 6 hours after seeding (i. – iii.) or were paced using pulsatile 12V/cm electric fields (iv. – vi.) at frequencies alternating between 1 Hz and 2 Hz. The diagrams show outlines of representative cell-occupied micropatterns spanning the range of observed motion between the basal tonic contraction (green) to the maximal contraction (red). The real-time videos corresponding to cases i. and iv. can be found in Movie S8 - S10. Cardiomyocytes showed heterogeneity in spreading behavior on “X” patterns, so pseudo-one-dimensional rod patterns were used (right). Here, the behavior was conserved, as all cells spread along this single dimension.

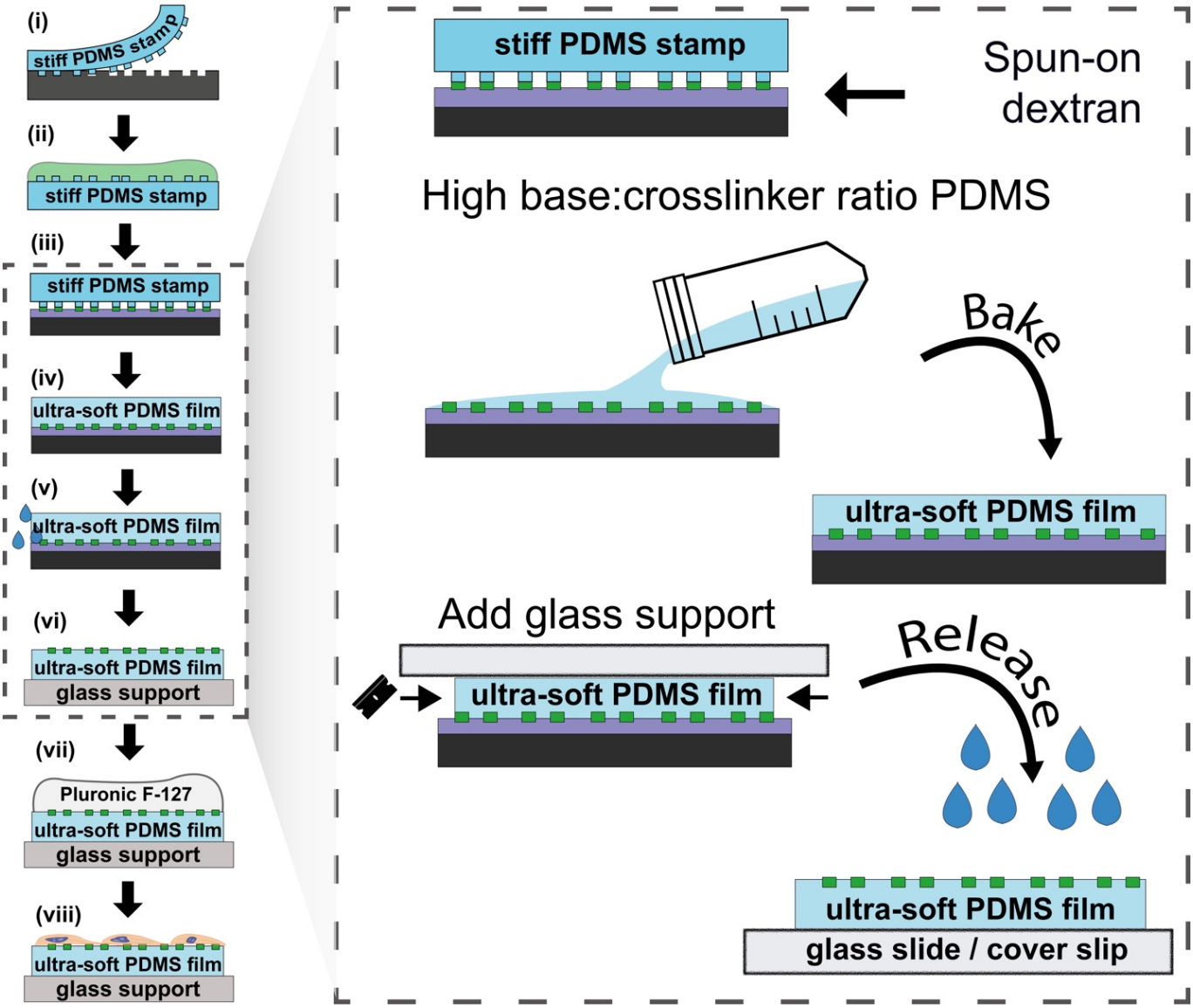


**Figure S9: Covalent bio-patterning on ultra-soft substrates via sacrificial dextran layers.**

(i) Cured PDMS stamps are demolded and (ii) incubated with biomolecule solution. (iii) After adsorption of the biomolecule is complete, the stamp is dried with air and used to stamp the biomolecule onto a dextran-coated silicon wafer that has been plasma-treated (30 s) for 5 mins. (iv) High base:crosslinker ratio PDMS is spin-coated over the stamped dextran-coated wafer and cured for ~7 days at 65 C. During this step, the thiol and amine functional groups present on the biomolecule are covalently coupled to the forming polymer network through a catalyst poisoning mechanism. This, in principle, enables the technique to be used with any peptide. (v) The PDMS film is cut away at the periphery revealing the sacrificial dextran layer. The sample is mounted with a glass support and submerged in saline to release the dextran layer yielding a glass-backed thin-film of PDMS with embedded patterns. (vi-viii) The sample is sterilized, chemically blocked and seeded with cells to

begin the experiment. This method of embedding proteins covalently directly into elastomers produces stable micropatterns that exhibit robust integrity under stresses form cells. As a direct comparison to Movies S1 and S2 which show cells contracting micropatterns fabricated via sacrificial layers, Movies S11 and S12 show how proteins that are adsorbed but not bound to the PDMS surface may be ruptured or peeled away from the surface. Such damage is not observed in any of the experiments presented in this work, all of which involved substrates made via sacrificial layers.

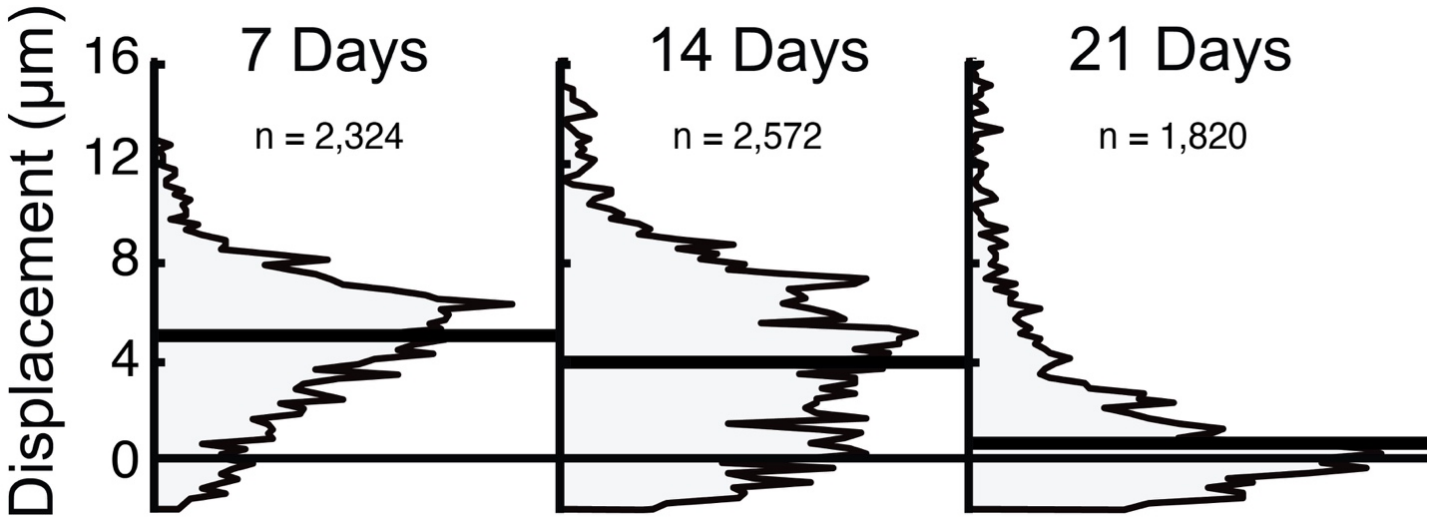


**Figure S10**: **Macrophages senesce following long term *in vitro* culture**.

Phagocytic forces produced by human monocyte-derived macrophages at different times after differentiation. Macrophages were seeded on hIgG cross patterns (50 μm diagonal, 10 μm bar thickness) for 6 hrs at 7 days, 14 days, or 21 days after initiating differentiation of monocytes. At 14 days, the phagocytic force response diminished substantially for a large portion of the macrophages and at 21 days, the large majority of macrophages applied little or no phagocytic force. For this reason, all macrophage experiments were performed using newly differentiated macrophages. We note there are visible differences in the distributions of the day 7 cells shown here and the cells in the experiment shown in Fig. 5 which are likely due to heterogeneity inherent to the different blood donors.

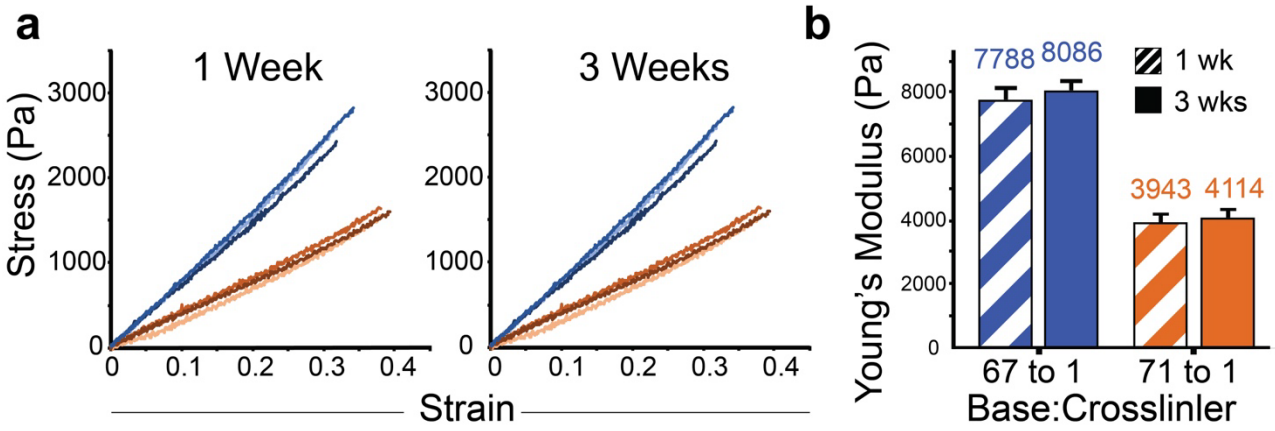


**Figure S11. Mechanical testing of PDMS used in macrophage experiments.**

PDMS samples at 67:1 and 71:1 base:crosslinker ratios were cured for 1 or 3 weeks, cut into cylinders and compression tested using an Instron 5564. Strain-stress curves **(a)** and geometric characteristics of the sample and tip were used to compute the stiffness. **(b)** The stiffness did not increase between 1 week and 3 weeks of curing at 65 C for either formulation. These values were used for approximating the forces generated by phagocytosing macrophages. We observe that on a macroscopic level, the material behaves elastically. Experiments with relaxing agents, such as blebbistatin (Fig. 2, Movie S3), formoterol (Fig. 3), and cytochalasin D (Fig. 6) all strongly indicate elasticity at the cellular scale, as the patterns are observed to restore size following inhibition of active contractile machinery.

**Table S1: Characteristics of patient donors of HASM cells**

## Patient pairs # 1-3

| Patient Pair # | 1 | 1 | 2 | 2 | 3 | 3 |
|---|---|---|---|---|---|---|
| Normal/Diseased | Asthmatic | Normal | Asthmatic | Normal | Asthmatic | Normal |
| Age | 38 | 21 | 14 | 19 | 29 | 30 |
| Race | Caucasian | Caucasian | Caucasian | Caucasian | Caucasian | Caucasian |
| Gender | Male | Male | Male | Male | Female | Male |
| BMI | 27.37 | 26.14 | 28.24 | 21.90 | 35.01 | 30.54 |
| ABO/Rh: | $B^+$ | A | B | A | O | $O^+$ |
| Cause of Death | Anoxia | Head Trauma | Anoxia | Head Trauma | Anoxia | Head Trauma |

## Patient pairs # 4-6

| Patient Pair # | 4 | 4 | 5 | 5 | 6 | 6 |
|---|---|---|---|---|---|---|
| Normal/Diseased | Asthmatic | Normal | Asthmatic | Normal | Asthma | Normal |
| Age | 20 | 22 | 21 | 18 | 44 | 38 |
| Race | African-American | African-American | Caucasian | Caucasian | Caucasian | Caucasian |
| Gender | Female | Female | Female | Female | Male | Male |
| BMI | 27.80 | 24.29 | 21.30 | 24.11 | 28.32 | 24.95 |
| ABO/Rh: | O | B | $O^+$ | A | $A^+$ | $O^-$ |
| Cause of Death | Anoxia | Head Trauma | Anoxia | Head Trauma | Anoxia | Head Trauma |

Patient pair numbers correspond to numbers listed on main text Fig. 3.

**Table S2: Summary of opsonin equalization procedure**

| Opsonin | Degree of labeling (mol dye per mol protein), *DOL* | Concentration used | Actual fluorescent intensity (a.u.), *FI* | Fraction of patterned protein that is labeled, $Frac_{labeled}$ | Relative surface molarity coefficient, $C_{sm}$* |
|---|---|---|---|---|---|
| BSA | 7 | 60 µg $mL^{-1}$ | 519 +/- 35 | 0.5 | 148.5 |
| Vitronectin | 6.25 | 30 µg $mL^{-1}$ | 963 +/- 45 | 1 | 154.1 |
| Fibrinogen | 6 | 10 µg $mL^{-1}$ | 1073 +/- 51 | 1 | 178.8 |

*The relative surface molarity coefficient is simply the measured fluorescent intensity normalized by the degree of labeling (moles dye per mole of opsonin) and adjusted for the proportion of opsonin that was fluorescently labeled.

$C_{sm} = (FI / DOL) \times frac_{labeled}^{-1}$

This coefficient reflects the relative amounts of each opsonin that were transferred to the substrates but does not indicate absolute molar quantity. The coefficients calculated for the substrates used in the opsonin-dependent phagocytosis experiment do not vary significantly between the three opsonins indicating similar molar quantities in the patterns of the final substrates that were used in experiments. Since only one-half of all present BSA was labeled with Alexa Fluor 488, the relative surface concentration was expected to be twice the amount predicted by the DOL. This factor of 2 is reflected in the relative surface molarity calculated for BSA.

## Movie captions

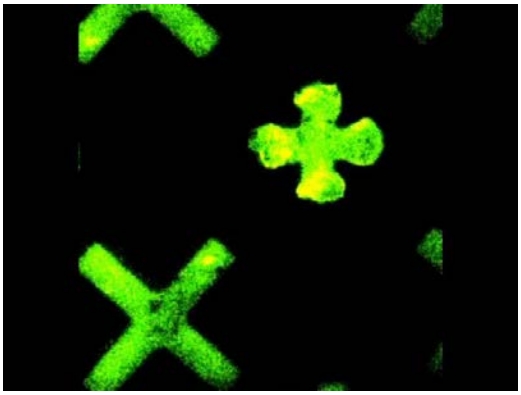

**Movie S1.** Fibronectin-fibrinogen patterns created using our sacrificial dextran method (Fig. S6). The adhered cell contracts the pattern but does not detach the protein from the surface. This also illustrates a typical symmetrically contracted pattern. Video duration is 8 hours.

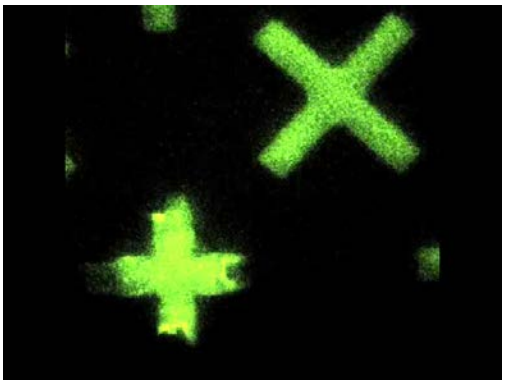

**Movie S2.** A second example of fibronectin-fibrinogen patterns created using our sacrificial dextran method (Fig. S6). The adhered cell contracts the pattern but does not detach the protein from the surface. This illustrates a second kind of typical symmetrical pattern contraction. Video duration is 8 hours.

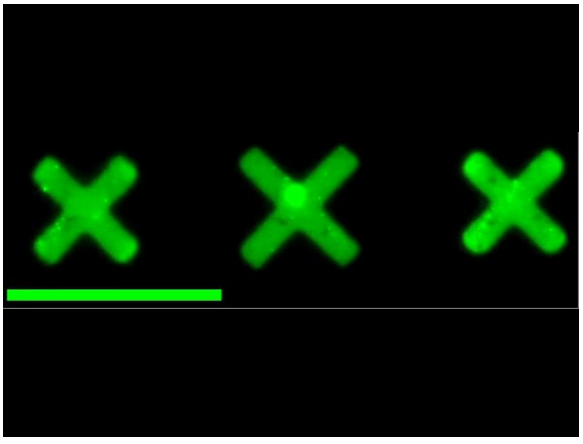

**Movie S3.** Patterns contracted by adhered HeLa cells relax after the addition of the myosin inhibitor, blebbistatin. Although the cells are still adhered resulting in some minimal pattern contraction, the original pattern shape is generally restored demonstrating the elasticity of the FLECS substrates. Video duration is 8 hours.

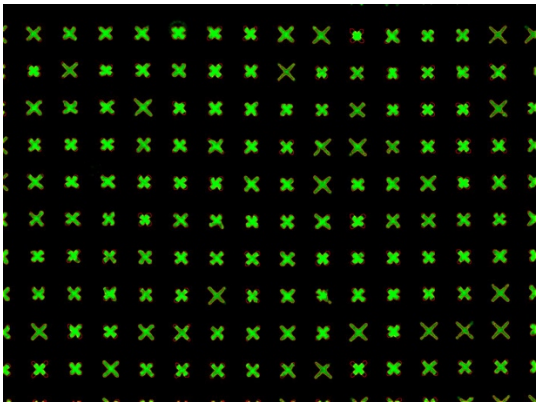

**Movie S4.** HASM cells treated with 1μM bradykinin are observed to contract significantly beyond tonic levels within 30 mins.

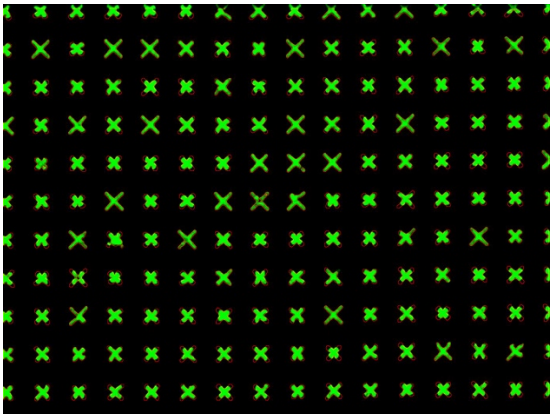

**Movie S5.** HASM cells treated with 100 nM endothelin-1 are observed to contract significantly beyond tonic levels within 30 mins.

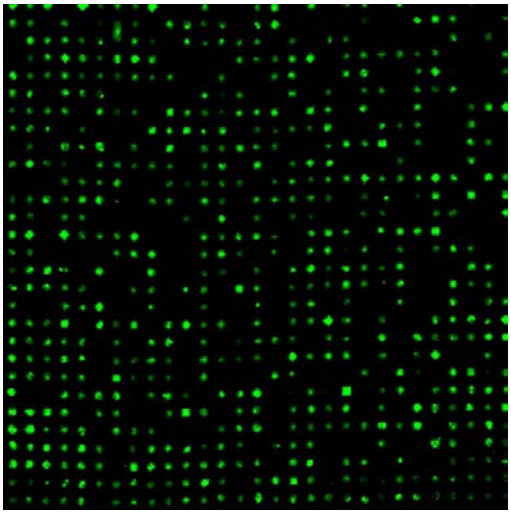

**Movie S6.** Visualization of calcium flux within HASM seeded on arrays of FLECS micropattern after the addition of Hist

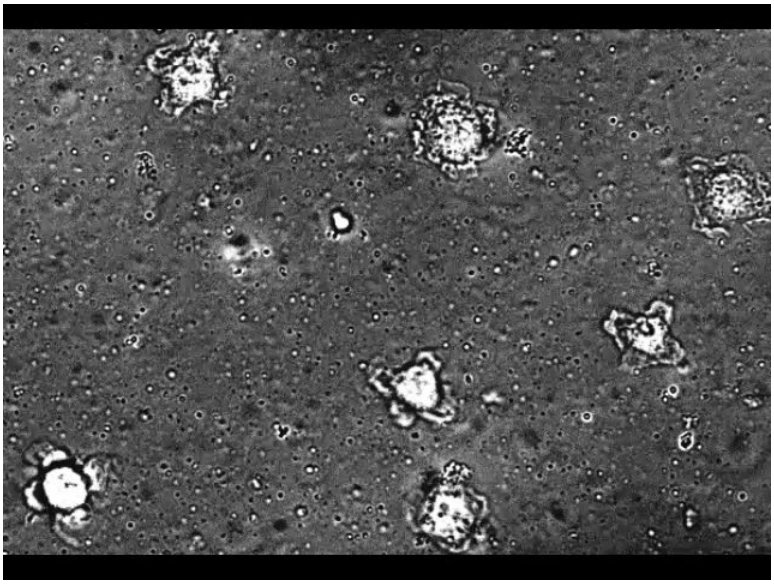

**Movie S7.** Time-lapsed video of human monocyte-derived macrophages engaged in frustrated phagocytosis of an IgG-opsonized patterned surface. A macrophage is seen making contact with an opsonized pattern and immediately adhering and initiating phagocytosis. Frustrated phagocytosis is sustained for over 6 hours. Video duration is 8 hours.

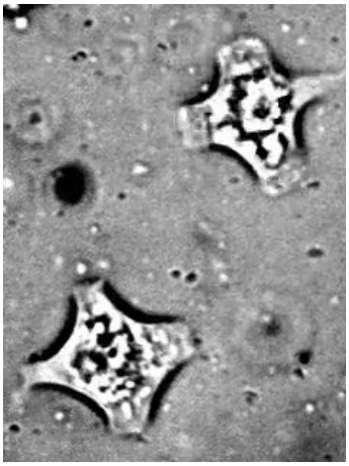

**Movie S8.** Representative video of a phasically contracting neonatal rat ventricular myocyte. Video is in real-time.

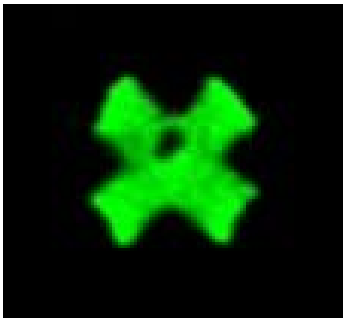

**Movie S9** Representative video of a pattern phasically contracted by an adhered and spontaneously beating neonatal rat ventricular myocyte. Video is in real-time.

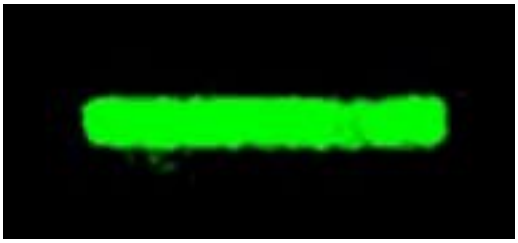

**Movie S10** Representative video of a pattern phasically contracted by an adhered and beating neonatal rat ventricular myocyte paced with pulsed electric fields at frequencies of 1 Hz and 2 Hz. Video is in real-time.

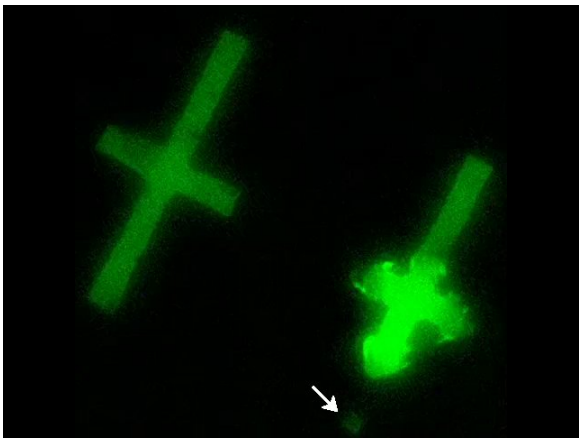

**Movie S11.** Fibronectin-fibrinogen patterns created using adsorption rather than our sacrificial dextran method. The adhered cell exerts enough force to detach the protein from the PDMS film, indicating that the commonly used adsorption technique is not robust enough for assays of highly contractile cells. Video duration is 8 hours. When using the sacrificial method of generating micropatterns, this is damage is not observed indicating resilience to the stresses generated by cells.

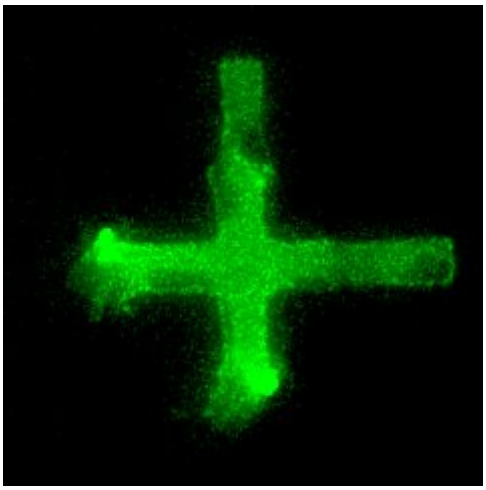

**Movie S12.** Second example of a fibronectin-fibrinogen patterns created using adsorption rather than our sacrificial dextran method that is damaged by cells. As with Movie S11, the adhered cell exerts enough force to detach the protein from the PDMS film, indicating that the commonly used adsorption technique is not robust enough for assays of highly contractile cells. Video duration is 8 hours. When emphasize that when using the sacrificial method of generating micropatterns, this is damage is not observed indicating resilience to the stresses generated by cells.